Submitted to Journal of
Chemical Physics

RECEIVED
LAWRENCE
RADIATION LABORATORY

UCRL-20713
Preprint

DOCUMENTS SECTION

LARGE ANGLE ELASTIC SCATTERING OF Ar^+ by He

M. H. Chiang, E. A. Gislason, B. H. Mahan,
C. W. Tsao, and A. S. Werner

June 1971

AEC Contract No. W-7405-eng-48

TWO-WEEK LOAN COPY

This is a Library Circulating Copy which may be borrowed for two weeks. For a personal retention copy, call Tech. Info. Division, Ext. 5545

UCRL-20713

LAWRENCE RADIATION LABORATORY
UNIVERSITY of CALIFORNIA BERKELEY

DISCLAIMER

This document was prepared as an account of work sponsored by the United States Government. While this document is believed to contain correct information, neither the United States Government nor any agency thereof, nor the Regents of the University of California, nor any of their employees, makes any warranty, express or implied, or assumes any legal responsibility for the accuracy, completeness, or usefulness of any information, apparatus, product, or process disclosed, or represents that its use would not infringe privately owned rights. Reference herein to any specific commercial product, process, or service by its trade name, trademark, manufacturer, or otherwise, does not necessarily constitute or imply its endorsement, recommendation, or favoring by the United States Government or any agency thereof, or the Regents of the University of California. The views and opinions of authors expressed herein do not necessarily state or reflect those of the United States Government or any agency thereof or the Regents of the University of California.

Large Angle Elastic Scattering of Ar^+ by He

M. H. Chiang, E. A. Gislason,* B. H. Mahan,
C. W. Tsao, and A. S. Werner

Department of Chemistry and Inorganic Materials Research
Division of the Lawrence Radiation Laboratory,
Berkeley, California

ABSTRACT

Measurement of accurate differential cross sections for systems of the type "heavy projectile--light target" are shown to be practical, provided measurements are restricted to large center-of-mass scattering angles θ. As an example, cross sections for the system Ar^+-He have been measured from $\theta = 60°$ to 180° in the energy range 2.7–9.1 eV. Using two-parameter repulsive potentials the results are inverted to yield a potential which reproduces the scattering at all energies. Dramatic evidence is given that potentials of the form $V(r) = K/r^s$ are unsatisfactory for fitting the intermolecular potential in the region of 1-10 eV. The potential derived from these experiments is an average of two molecular potentials, since both the $X^2\Sigma$ and $A^2\pi$ states of Ar^+-He correlate to ground state atoms. Comparisons are made with theoretical estimates of the two molecular potentials and with the Ar-He^+ and Ar-He potentials.

---

*Present address: Department of Chemistry, University of Illinois at Chicago Circle, Chicago, Illinois.

INTRODUCTION

The study of intermolecular forces in molecular beam scattering experiments has been quite fruitful in recent years. This is especially true for low energy experiments which give information about the attractive region of the intermolecular potential.[1] Short range repulsive forces have been studied by a number of methods. One involves the measurement of elastic differential cross sections at small angles but high energy where repulsive interactions dominate.[2] A closely related technique is the determination of high energy total cross sections as a function of energy, a method pioneered by Amdur and coworkers.[3] Both techniques, however, involve measurements of scattering at very small angles where the angular distributions are changing rapidly with angle. Thus, substantial corrections must be made for the finite angular resolution of the apparatus before comparing with theory. Measurements at larger center of mass scattering angles, where the resolution problem is not so severe, have been made in low-energy crossed beam studies of elastic scattering. These also give direct information about the repulsive potential. Again, however, the analysis in these experiments can be quite complicated since one beam usually is not velocity selected and may have a large angular width. An additional problem with these experiments is that the elastic differential cross section is many orders of magnitude smaller at 180° than at 0°, and signal-to-noise problems can become quite important.

In this work measurements are presented of the differential cross section from 60° to 180° in the center of mass coordinate

system for the Ar^+-He system. The relative kinetic energy has been varied from 2.7eV to 9.1eV. The experiments make use of the fact that a heavy projectile scattered elasticly by a light target must remain in a region of velocity space where it can be detected quite easily. To obtain a differential cross section it is necessary only to velocity select the beam particles before and after collision and measure the intensity at the accessible laboratory deflection angles. We feel this method has many advantages which make it a promising source of data on intermolecular forces: (a) Localization of the scattering due to the relative masses of projectile and target greatly increases the density of scattered product in laboratory velocity space. The signal at the detector is correspondingly larger. This localization also permits use of a scattering cell with its concommitant improvement in signal-to-noise; (b) In many cases the velocity of the target gas can be neglected in the data analysis, either by use of high energy beams (as in the present case) or by cooling down the gas to sufficiently low temperatures; (c) Restriction of the experiments to large center of mass angles neatly avoids the problem of angular resolution because the scattering varies slowly with angle in this region. For example, the Ar^+-He differential cross section varies by at most a factor of six in going from 60° to 180°. Because of this we feel that no corrections need be made to our data, even though the angular resolution of our apparatus in the center of mass is only 23°.

A number of other kinds of molecular beam experiments have found this localization of scattered intensity due to favorable

mass ratios quite useful. For example, the Ar^+-He measurements discussed here were originally made to compare with a study of the reactive and nonreactive scattering in the system $Ar^+ + D_2$.[4] For this and other ion-molecule reactions involving H_2 and D_2 the scattering at all center of mass angles is easily detected, and very complete studies have been made in a number of laboratories.[5] A second example is the recent molecular beam studies of vibrational excitation in small impact parameter collisions for the systems Li^+-H_2[6] and K^+-H_2.[7]

After a brief description of the experimental apparatus, the conversion of measured intensities into absolute differential cross sections is discussed in some detail. Because of experimental uncertainty in the data, no attempt is made to directly invert the data to obtain potentials. Rather, the measured cross sections are compared to the scattering expected from three simple repulsive potentials. The major problem in interpreting the scattering in the system Ar^+-He is that two states, the $X^2\Sigma$ and the $A^2\Pi$, correlate to separated ground state atoms. It is shown, however, that in the region near $\theta = 180°$ scattering by two potential curves is equivalent to the scattering by one average or "effective" potential, and simple rules are given for finding this effective potential. We have determined the effective potential for Ar^+-He in the region of 0.5eV to 9eV. A theoretical estimate of the $X^2\Sigma$ and $A^2\Pi$ potential curves has been reported by Smith et al,[8] and our results are in reasonably good agreement with them. A considerable amount is known about the related systems Ar-He^+[2,9,10] and Ar-He,[1a,3,10,11] and a com-

parison of the three diatomics is quite instructive.

EXPERIMENTAL AND DATA ANALYSIS

The apparatus used for this work has been described elsewhere.[12] Briefly, it consists of a conventional electron bombardment source, a magnetic mass spectrometer for preparing the ion beam with a well-defined energy, a scattering cell which contains the scattering gas, and the final analysis and detection system. The gas pressure is monitored by a capacitance manometer. The exit slit of the scattering cell is mounted on a rotating lid, so that the laboratory scattering angles can be varied. Ions which emerge from the slit pass successively into an electrostatic energy analyzer, a quadrupole mass filter, and an ion counter. Thus the intensity of scattered ions is known as a function of laboratory angle and energy. The angular resolution (in the center of mass) of the apparatus for this mass ratio is about 23°; the energy resolution is not quite good enough to observe transitions between the $^2P_{3/2}$ and $^2P_{1/2}$ states of Ar^+ (0.18eV apart).

The next step is to convert the measured laboratory intensities into center-of-mass intensities. The Ar^+ velocity in the lowest energy experiment was 1.2×10^6 cm/sec, whereas room temperature helium has an average velocity of 1.1×10^5 cm/sec. Thus it is reasonable to neglect the helium velocity in the conversion, and any laboratory vector $\underset{\sim}{v}$ can be converted into a center-of-mass vector $\underset{\sim}{u}$ by the expression

$$\underset{\sim}{v}-\underset{\sim}{u} = \underset{\sim}{V}_{cm} = (40/44)\ \underset{\sim}{v}_o. \qquad (1)$$

Here $\underset{\sim}{V}_{cm}$, the center-of-mass velocity vector, is parallel to the

Ar^+ beam velocity $\underset{\sim}{v}_o$, since we have neglected the He velocity. The two specific differential cross sections $I(\underset{\sim}{v})$ and $I(\underset{\sim}{u})$ are functions of both angle and speed, and it can be shown (see Ref. 4 for details) that

$$I(\underset{\sim}{v}) = I(\underset{\sim}{u}). \tag{2}$$

The cross sections are normalized so that

$$\sigma = \int I(\underset{\sim}{v})d\underset{\sim}{v} \tag{3}$$
$$= \int I(\underset{\sim}{u})d\underset{\sim}{u},$$

where σ is the total scattering cross section. In this work we are chiefly interested in the center-of-mass differential cross section $I(\theta)$, calculated from

$$I(\theta) = \int_0^\infty I(\underset{\sim}{u})u^2 du. \tag{4}$$

Our experiments measure the scattered intensity at a large number of laboratory angles and energies. Each intensity is converted into a value of $I(\underset{\sim}{u})$ using Eq. (2). The values are then integrated numerically using Eq. (4) to obtain $I(\theta)$ at 20 degree spacings. For example, the differential cross at the nominal angle θ=160° is obtained using all values of $I(\underset{\sim}{u})$ which fall between 150° and 170°. Assuming $I(\theta)$ is approximately linear in this 20 degree region, the value obtained should be quite reliable. This method will certainly break down at small angles, however, so we have restricted ourselves to angles greater than 50°.

The primary data for this work has been presented earlier,[4] including two contour maps of $I(\underset{\sim}{u})$ for Ar^+-He scattering as well as the differential cross sections $I(\theta)$ at relative energies of 2.75eV, 4.57eV, 6.83eV, and 9.08eV. The nonreactive scattering

of Ar^+ by He was originally done for comparison with the reactive system Ar^+-D_2. In fact, the absolute magnitudes of $I(\theta)$ for both the Ar^+-He and Ar^+-D_2 systems were obtained by normalizing our reactive scattering data to a total reactive cross section measured by Robb et al.[13] This normalization procedure is described in more detail in Ref. 4. Here it suffices to say that we estimate the absolute values of $I(\theta)$ for the Ar^+-He system to be uncertain by 10 to 15%.

For the sake of comparison with theoretical calculations it is best to present the data in a different format from Ref. 4. First, in Fig. 1 the differential cross sections at $\theta=180°$ are presented as a function of relative kinetic energy. The data at other angles are presented in Fig. 2 as the ratio $I(\theta)/I(\pi)$ plotted against $(\pi-\theta)^2$. Each point in Fig. 1 may be in error by 15% to 20% when the random experimental error is added to the possible nonrandom error due to the normalization procedure. Points in Fig. 2 will not show any effect of the normalization procedure, but in extreme cases we estimate each point could be uncertain by 15%, simply due to random experimental errors.

RESULTS AND DISCUSSION

Since the data have a substantial amount of uncertainty, it would be pointless to try to directly invert the cross sections to obtain a potential. Rather we intend to compare the scattering with that predicted for three simple repulsive potentials, namely the inverse power potential

$$V = K/r^s, \tag{5}$$

the exponential repulsive potential

$$V = A \exp(-r/a), \tag{6}$$

and the shielded Coulomb potential

$$V = A(a/r)\exp(-r/a). \tag{7}$$

For these particular experiments we are almost certainly safe ignoring the long-range attractive part of the potential. In our lowest energy experiment the potential energy at the turning point for a collision with $\theta=60°$ is 1.2eV, and it is correspondingly larger for wider-angle collisions. For comparison, the well depth of the Ar^+-He system is most likely 0.1 eV or smaller.

The analysis is complicated considerably by the fact that Ar^+ and He will interact along two potential curves, the $X^2\Sigma$ and the $A^2\Pi$. Statistical weighting indicates that two thirds of all the collisions will occur on the $^2\Pi$ curve and one third on the $^2\Sigma$ curve. Since there is no way for us to distinguish the scattering from the two curves, we must analyze the results assuming a single potential is responsible for all scattering. The potential obtained in this way will be a weighted average of the $^2\Sigma$ and $^2\Pi$ potentials. A further problem is the spin-orbit splitting between the $^2P_{3/2}$ (lower) and $^2P_{1/2}$ (upper) states of Ar^+ of 1432 cm^{-1} or 0.18eV. Thus the $^2\Pi$ potential at small separations is also split into two states. Collision induced transitions between the two states of Ar^+ have been directly observed in Ar^+-D_2 collisions by Moran and Cosby.[14] In addition, deconvolution of the Ar^+-He data taken in our laboratory indicates that for head-on collisions ($\theta=180°$) the two states of Ar^+ are substantially mixed by collisions. This suggests that the two $^2\Pi$

states cross, or at least remain quite close at small internuclear separation. Since the electrostatic energy analyzer will not clearly separate these two states, no effort is made to distinguish them in the data analysis. All the intensity is integrated together to give $I(\theta)$. For these reasons we will ignore the effect of spin-orbit coupling as relatively unimportant and will talk about a single $^2\Sigma$ state and a single $^2\Pi$ state. In reality the latter represents an average of the two $^2\Pi$ states.

In a companion paper[15] we examined the scattering near $\theta=180°$ for the three potentials given earlier. For the inverse power potential in Eq. (5) we can write

$$I(\theta) = (\sin\theta)^{-1}(\pi-\theta)(K/E)^{2/s}i(s)[1-h(s)(\pi-\theta)^2+ \ . \ . \ . \ ], \quad (8)$$

where the functions $i(s)$ and $h(s)$ are tabulated in Ref. 15. Thus a plot of $I(\theta)/I(\pi)$ will give s; once s is known, $I(\pi)$ will yield K. One drawback of this potential is that s must be known before even the units of K, let alone the magnitude, can be determined. If the scattering arises from two potentials, one with potential constants (L,t) and the other with (M,u), with statistical weighting factors x and y (x+y=1), the total differential cross section can be put in a form similar to Eq. (8), but now

$$I(\pi)=(K/E)^{2/s}i(s)=x(L/E)^{2/t}i(t)+y(M/E)^{2/u}i(u) \quad (9)$$

and

$$h(s)=[x(L/E)^{2/t}i(t)h(t)+y(M/E)^{2/u}i(u)h(u)]/I(\pi). \quad (10)$$

Thus, near $\theta=180°$ (typically, to $\theta=60°$) the scattering of two inverse power potentials is equivalent to the scattering of one "effective" inverse power potential, and Eqs. (9) and (10) indicate how the "effective

potential parameters K and s are to be found. Both K and s depend on the potential constants L, t, M, and u, the weighting factors x and y, and the relative energy E. Even though the exponents t and u are constant, the value of s will, in general, change with E. At low energies s will approach the smaller of t and u; at high energy s will approach the larger as would be expected. The results are considerably simpler for the special case t=u. Then Eqs. (9) and (10) yield

$$s=t=u, \tag{11}$$
$$K = [xL^{2/s} + yM^{2/s}]^{s/2}.$$

Clearly, K and s are independent of E in this case.

Scattering by either an exponential repulsive potential (Eq. (6)) or a shielded Coulomb potential (Eq. (7)) yields similar results. In both cases the differential cross section near $\theta=180°$ can be written

$$I(\theta)=(\sin\theta)^{-1}(\pi-\theta)a^2 j(A/E)[1-H(A/E)(\pi-\theta)^2 + \ldots]. \tag{12}$$

Appropriate formulas for the functions $j(A/E)$ and $H(A/E)$ are given in Ref. 15 for both potentials. We see from Eq. (12) that a plot of $I(\theta)/I(\pi)$ will give A/E and thus A; subsequently, a can be obtained from $I(\pi)$. If two particles scatter off two exponential repulsive potentials (or two shielded Coulomb potentials) which have potential constants (B,b) and (D,d) and weighting factors x and y (x+y=1), the total differential cross section near $\theta=180°$ can be put in a form similar to Eq. (12), but now

$$I(\pi) = a^2 j(A/E) = xb^2 j(B/E) + yd^2 j(D/E) \tag{13}$$
$$H(A/E) = [xb^2 j(B/E)H(B/E) + yd^2 j(D/E)H(D/E)]/I(\pi). \tag{14}$$

Thus near $\theta=\pi$ the scattering by two exponential potentials (or two shielded Coulomb potentials) is equivalent to the scattering by one "effective" exponential repulsive potential (one "effective" shielded Coulomb potential). The parameter A and a for this "effective" potential can be obtained from Eqs. (13) and (14). In general, both A and a will be functions of E even though B, b, D, and d are not.

These considerations focus the problem in interpreting the scattering for the Ar^+-He system. Even if both potential curves can be approximated by the simple, two-parameter potentials in Eqs. (5)-(7), the experimental cross sections will not give these potential parameters directly. Rather, at each energy the data gives the "effective" potential which reproduces the combined scattering of the two real potentials at that energy. The analysis is simplified somewhat if we make the assumption that the ratio of the $^2\Pi$ and the $^2\Sigma$ potentials is roughly constant (independent of r) in the region of our experiments. As we will see, there is some theoretical evidence for this, and it seems reasonable because the relevant atomic orbitals of Ar^+ should have a similar r-dependence. Assuming the two potentials can be approximated by inverse power potentials, then the exponents must be the same. This is the special case covered by Eq. (11). If instead, the two real potentials are approximated by exponential repulsive (or shielded Coulomb) potentials, the two fall-off lengths must be the same. Calculations using Eq. (13) then indicate that

$a \approx b = d$,

provided that B and D are not greatly different.

Exact differential cross sections have been computed for the three potentials in Eqs. (5)-(7). The details are given in the companion paper.[15] In Figs. 1 and 2 these cross sections for the exponential repulsive potential are compared with the experimental results. Within experimental error all the data in Fig. 2 can be fit by A=220±20eV. We then used this value to generate the curves in Fig. 1. Combining the results from these two Figures, we find that all of our data can be fit by the potential

$$V(r)=(220\pm20\text{eV})\exp[-r/(0.39\pm0.03\text{Å})] \tag{15}$$

In Figures 3 and 4 the exact calculations for a shielded Coulomb potential are compared with the experimental data. All the data in Fig. 4 can be fit by A=190±40, and the value A=190 was used for the curves in Fig. 3. From this we can see that the potential

$$V(r)=(190\pm40\text{eV})(0.55\text{Å}/r)\exp(-r/0.55\text{Å}) \tag{16}$$

also fits the data within experimental error. The fall-off length of 0.55A is uncertain by about ±0.04Å. These two potentials are shown in Fig. 5. Their range of validity is from 9.1eV, the highest experimental energy, down to about 0.5eV. Again it should be stressed that although the experimental cross sections can be fit by a single potential, there are in fact two potential curves contributing to the scattering.

The cross sections computed for inverse power potentials are shown in Fig. 6, along with the data. The values of the exponent s which fit the data may seem surprisingly small, but are in fact consistent with the potentials given in Eqs. (15) and (16). A more serious problem is that the value of s is changing rapidly with energy, but in an interesting manner. As discussed earlier, if the two potentials for the Ar^+-He system can be approximated by inverse power potentials with exponents t and u, then at low energies the scattering will be dominated by the longer-ranged of the two potentials (i.e., the one with the smaller exponent). The "effective" value of s which fits the data will then decrease with decreasing energy, approaching the smaller of t and u in the limit. As shown in Fig. 6, however, the "effective" exponent s actually increases with decreasing energy! We must conclude then that the inverse power potential is a very poor approximation for at least one, and almost certainly both, of the Ar^+-He potentials. In fact, the decrease of the "effective" value of s with increasing energy is reasonable, considering that the potential must approach the r^{-1} form at very high energies. These data are perhaps the most dramatic evidence to date of the failure of inverse power potentials to fit the repulsive part of intermolecular potentials. Both the exponential repulsive and shielded Coulomb potentials are much more satisfactory in fitting intermolecular potentials over long regions of internuclear separation. Over short regions of r, of course, the true potential can be approximated by an inverse power potential. Thus, if we invert the data in Fig. 6, treating each experiment separately, the inverse power potentials obtained are in satisfactory agreement with the exponential and shielded Coulomb potentials derived earlier.

A theoretical estimate of $^2\Sigma$ and $^2\pi$ potential curves for Ar^+-He has been reported in the literature by Smith et al.[8] They scaled the $^2\Sigma$ and $^2\pi$ curves computed for the Ne^+-He system by H. H. Michels (unpublished). We have fit the two curves in their figure by the following equations:

$$(A^2\pi)\ V(r) = (1194\text{eV})\exp(-r/0.277\text{Å}) \tag{17}$$

$$(X^2\Sigma)\ V(r)=(563\text{eV})\exp(-r/0.277\text{Å}). \tag{18}$$

These curves are compared in Fig. 5 with the potentials in Eqs. (15) and (16). Apparently, the calculated fall-off lengths are the same for both states, but smaller than our experimental value of 0.39Å. However, the preexponential factors are such that these theoretical curves agree reasonably well with the "effective" potential determined in these experiments. A better comparison can be made by using the two theoretical potentials and the analysis in Eqs. (12)-(14) to predict what "effective" potential should be determined experimentally. Recalling that the $A^2\pi$ state has a weight of 2/3, the $X^2\Sigma$ a weight of 1/3, the result is

$$V(r)=(1007\text{eV})\exp(-r/0.277\text{Å}). \tag{19}$$

This potential is shown as the dotted line in Fig. 5. Assuming the experimental results are uncertain by 15 or 20%, we see that the agreement is quite good over most of the range of r. The experimental results suggest, however, that the fall-off length of the potential

is somewhat larger than the predicted value of 0.277Å.

It is of interest to compare the potential curves for the three systems Ar^+-He, Ar-He^+, and Ar-He. All three have shallow van der Waals wells -- the best available values for Ar-He^+ and Ar-He are given in Table I. We can estimate the wells for the two Ar^+-He states by combining the repulsive potential in Eq. (15) with the attractive ion-induced dipole potential which will dominate at large r:

$$V_{id}(r) = -1/2\alpha e^2/r^4,$$

where e is the electronic charge and α is the polarizability of He. With α=0.206Å[3] [16] the minimum lies at 4.9Å, far larger than the values for Ar-He^+ and Ar-He (see Table I). For comparison we also computed the well depth and location using Eq. (19) in combination with the ion-induced dipole potential. The minimum at 3.5Å is closer to the other two diatomics. In either case, the well for the Ar^+-He system is much shallower than for the Ar-He^+; this is to be expected because Ar has a much larger polarizability than He. In the repulsive region of 1-10eV we can compare the results for Ar-He^+ [2] and Ar-He [11] with our results for Ar^+-He in Eq. (15). This is done in Fig. 7 by arbitrarily superimposing the asymptotic energies for all three systems. The three potentials are remarkably similar in this region.

SUMMARY

The determination of intermolecular potentials is seen to be

feasible for systems where the projectile is much heavier than the target atom. Although the mass ratios make the center-of-mass angular resolution much poorer than when the projectile is light, this can be compensated for by only measuring angular distributions at large center of mass angles. Here the cross section varies slowly with angle, and, as we have seen, the analysis of the data is quite simple. The "effective" potential we obtained for the Ar^+-He molecule, an average of the $^2\Sigma$ and $^2\pi$ potentials, is quite reasonable and in fairly good agreement with the estimates of Smith et al.[8] It is expected that the general method described can be applied to many other systems.

ACKNOWLEDGEMENTS

This work was supported by the U.S. Atomic Energy Commission. E. A. G. acknowledges a postdoctoral fellowship from the National Center for Air Pollution Control of the U. S. Public Health Service.

Table I. -- Comparison of Potential Curves for Ar^+-He, Ar-He^+, and Ar-He

	Ar^+-He	Ar-He^+	Ar-He
Well Depth (eV)	-0.0018[a] (-0.0066)[b]	-0.15[c]	-0.0022[d]
Internuclear Separation at Minimum (Å)	4.9[a] (3.5)[b]	3.0[c]	3.4[d]

[a] Determined using Eq. (15) of the text plus the ion-induced dipole potential.

[b] Determined using Eq. (19) of the text plus the ion-induced dipole potential.

[c] From Ref. 2.

[d] From Ref. 1a.

REFERENCES

1. Recent reviews include: (a) R. B. Bernstein and J. T. Muckerman, Advan. Chem. Phys. 12, 389 (1967); (b) Ch. Schlier, Ann. Rev. Phys. Chem. 20, 191 (1969).

2. See, for example, F. T. Smith, R. P. Marchi, D. C. Lorents, W. Aberth, and O. Heinz, Phys. Rev. 161, 31 (1967).

3. For reviews, see: (a) E. A. Mason and J. T. Vanderslice in Atomic and Molecular Processes, D. R. Bates, Ed., (Academic, New York, 1962), p. 663; (b) I. Amdur and J. E. Jordan, Advan. Chem. Phys. 10, 29 (1966).

4. M. Chiang, E. A. Gislason, B. H. Mahan, C. W. Tsao, and A. S. Werner, J. Chem. Phys. 52, 2698 (1970).

5. The Ar^+-D_2 system is a good example. See Ref. 4 and work cited therein. Also, P. M. Hierl, Z. Herman, and R. Wolfgang, J. Chem. Phys. 53, 660 (1970).

6. J. Schottler and J. P. Toennies, Z. Physik 214, 472 (1968).

7. P. F. Dittner and S. Datz, J. Chem. Phys. 49, 1969(1968).

8. F. T. Smith, H. H. Fleischmann, and R. A. Young, Phys. Rev. A2, 379 (1970).

9. J. Baudon, M. Barat, and M. Abignoli, J. Phys. B: Atom. Molec. Phys. 3, 207 (1970).

10. V. K. Nikulin in Sixth International Conference on the Physics of Electronic and Atomic Collisions (MIT Press, Cambridge, Mass., 1969), p. 520.

11. R. L. Matcha and R. K. Nesbet, Phys. Rev. 160, 72 (1967).

12. W. R. Gentry, E. A. Gislason, B. H. Mahan, and C. W. Tsao, J. Chem. Phys. 49, 3058 (1968).

13. J. B. Homer, R. S. Lehrle, J. C. Robb, and D. W. Thomas, Nature 202, 795 (1964).

14. T. F. Moran and P. C. Cosby, J. Chem. Phys. 51, 5724 (1969).

15. E. A. Gislason, J. Chem. Phys. 00, 000 (1971).

16. E. W. Rothe and R. B. Bernstein, J. Chem. Phys. 31, 1619 (1959).

FIGURE CAPTIONS

Figure 1. Differential cross section at π radians versus relative kinetic energy. The circles are experimental data. The curves are computed for the potential $V=A\exp(-r/a)$ with A= 220eV.

Figure 2. The ratio of $I(\theta)$ to $I(\pi)$, the differential cross section at π radians, versus $(\pi-\theta)^2$. The individual points are experimental data. The curves are computed for the potential $V=A\exp(-r/a)$.

Figure 3. $I(\pi)$ versus relative energy. The circles are experimental data. The curves are computed for the potential $V=A(a/r)\exp(-r/a)$ with A=190eV.

Figure 4. $I(\theta)/I(\pi)$ versus $(\pi-\theta)^2$. Individual points are experimental data. The curves are computed for the potential $V=A(a/r)\exp(-r/a)$.

Figure 5. The potentials V(r) for Ar^+-He. The two dash-dot curves are the theoretical estimates of Smith et al.[8] The solid and the dashed curves are experimental results -- Eqs. (15) and (16) of the text, respectively. The dotted curve is a weighted average of the two theoretical curves due to Smith -- Eq. (19) of the text.

Figure 6. $I(\theta)/I(\pi)$ versus $(\pi-\theta)^2$. Points are experimental data. The curves are computed for the potential $V=K/r^s$.

Figure 7. Comparison of the intermolecular potentials for Ar^+-He, Ar-He^+, and Ar-He. The Ar^+-He curve is from this work -- Eq. (15) of the text. The Ar-He^+ curve was derived by Smith et al from experimental data in Ref. 2. The Ar-He potential was computed by Matcha and Nesbet in Ref. 11. The curves have been shifted so that V(r) is zero at infinity in each case.

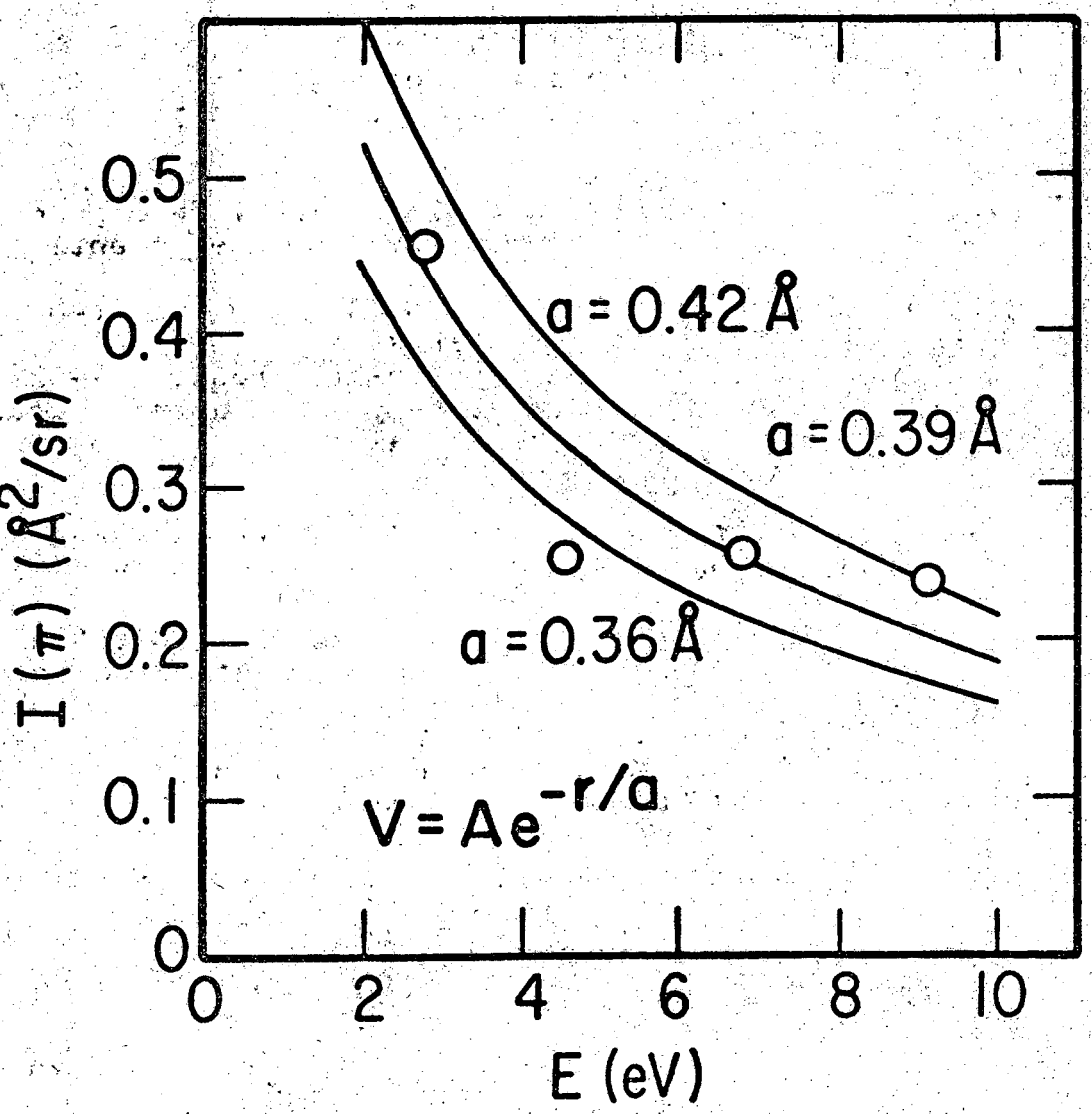

Fig. 1

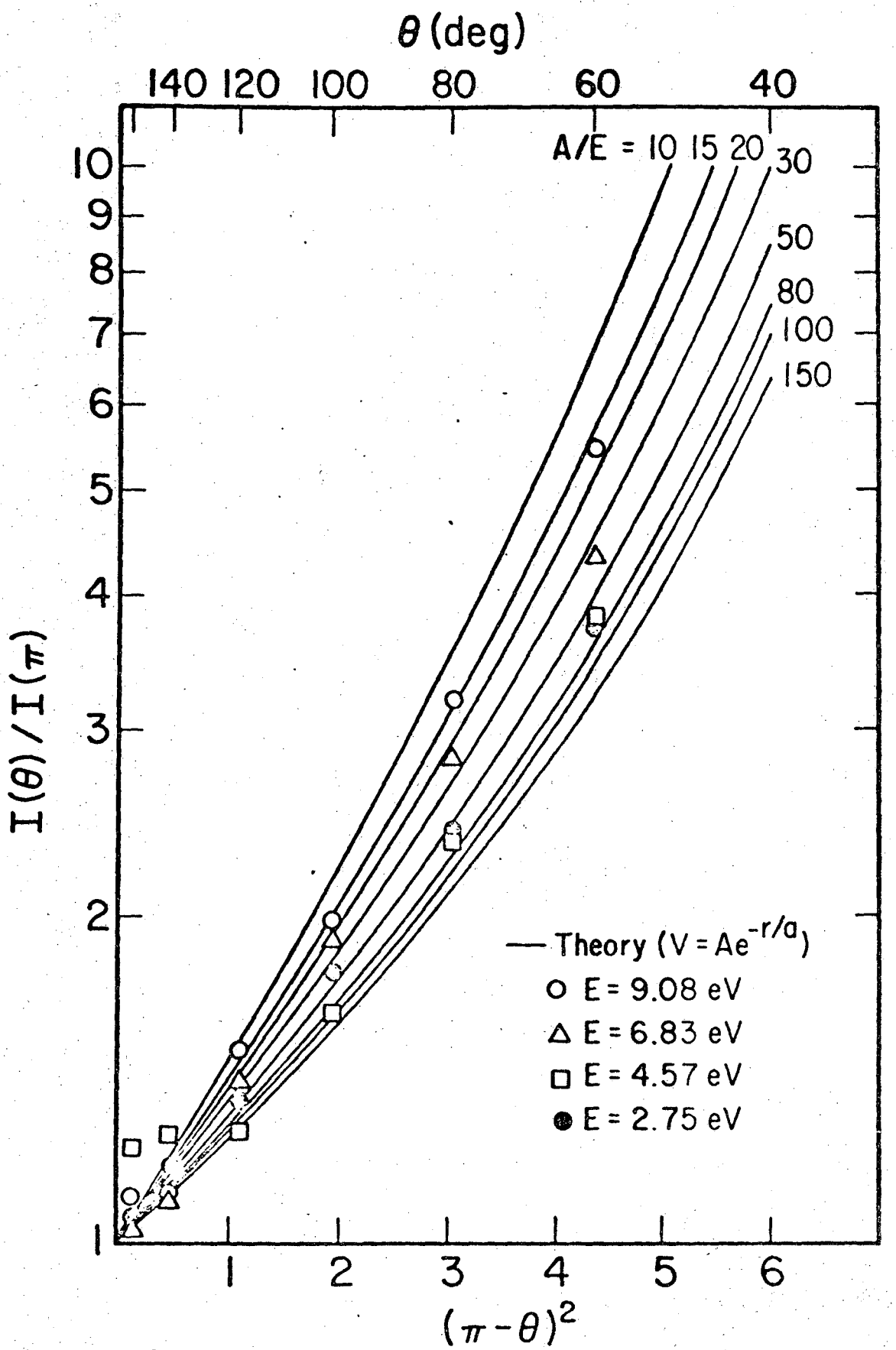
θ (deg)
140 120 100 80 60 40
A/E = 10 15 20 30
50
80
100
150
10
9
8
7
6
5
4
3
2
1
I(θ)/I(π)
— Theory (V = Ae^-r/a)
○ E = 9.08 eV
△ E = 6.83 eV
□ E = 4.57 eV
● E = 2.75 eV
1 2 3 4 5 6
(π-θ)²

Fig. 2

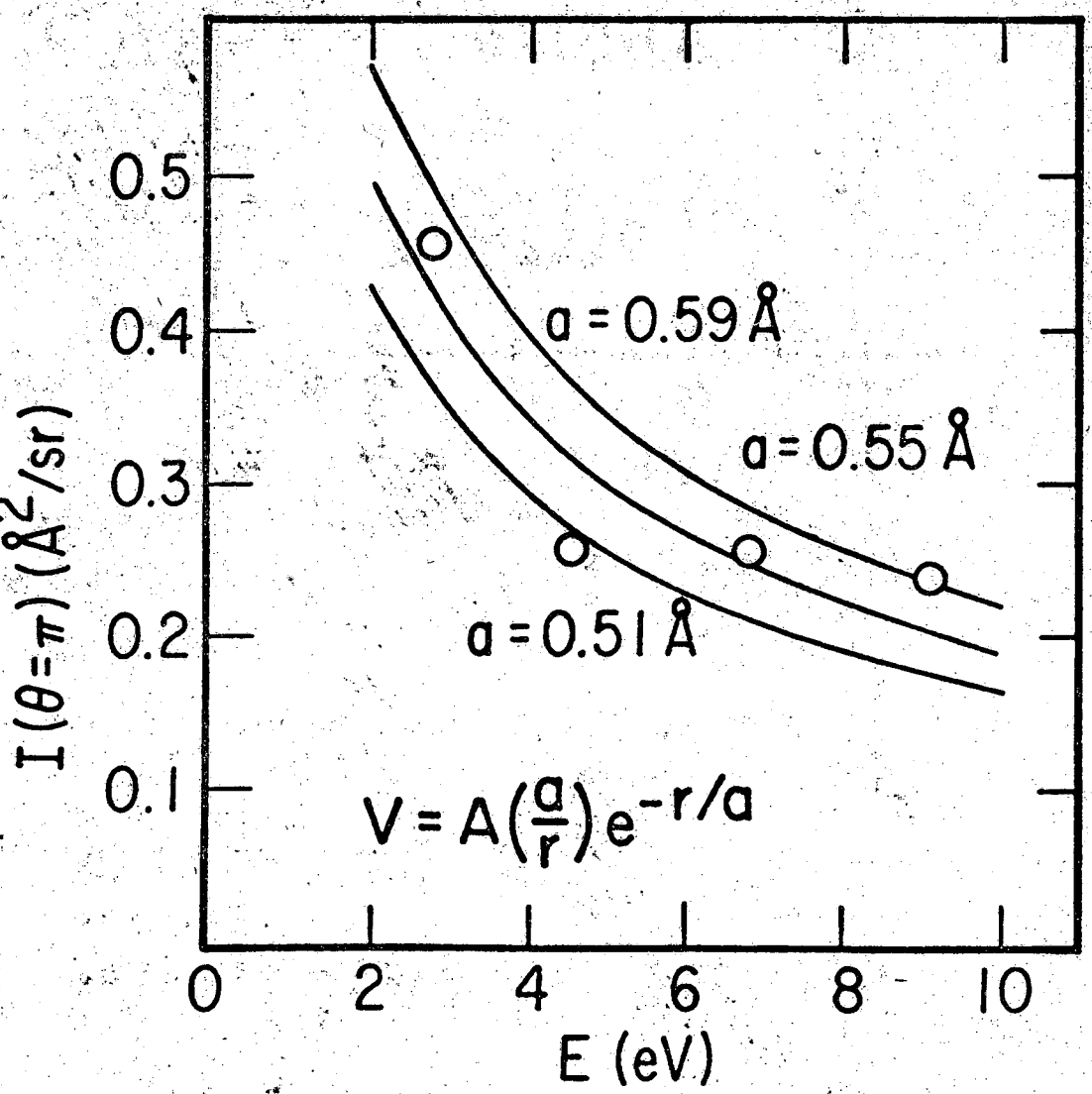

Fig 3

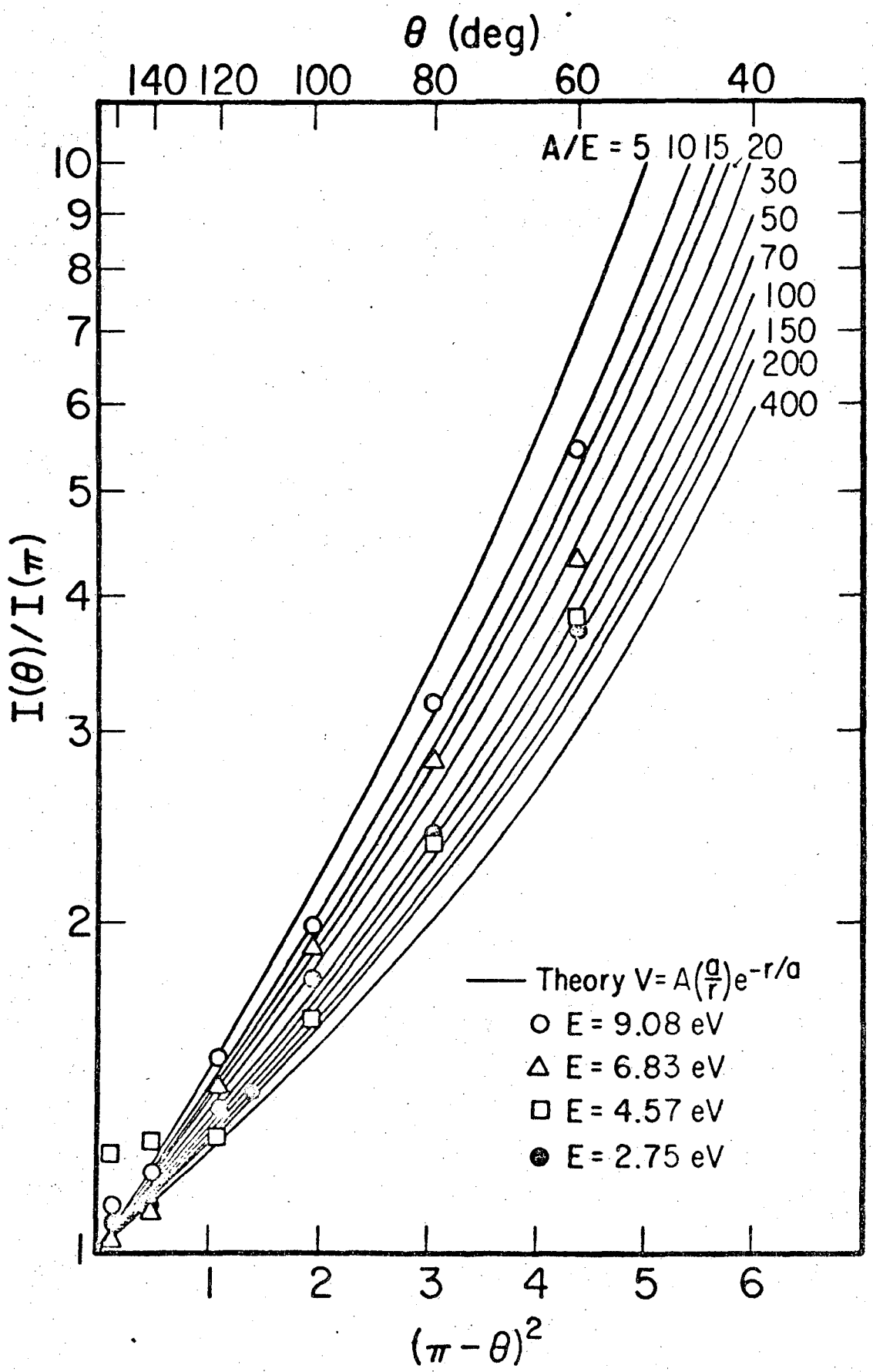
θ (deg)
140 120 100 80 60 40
A/E = 5 10 15 20
30
50
70
100
150
200
400
I(θ)/I(π)
10
9
8
7
6
5
4
3
2
1
Theory V= A(a/r)e^-r/a
E = 9.08 eV
E = 6.83 eV
E = 4.57 eV
E = 2.75 eV
1 2 3 4 5 6
(π − θ)^2

Fig. 4

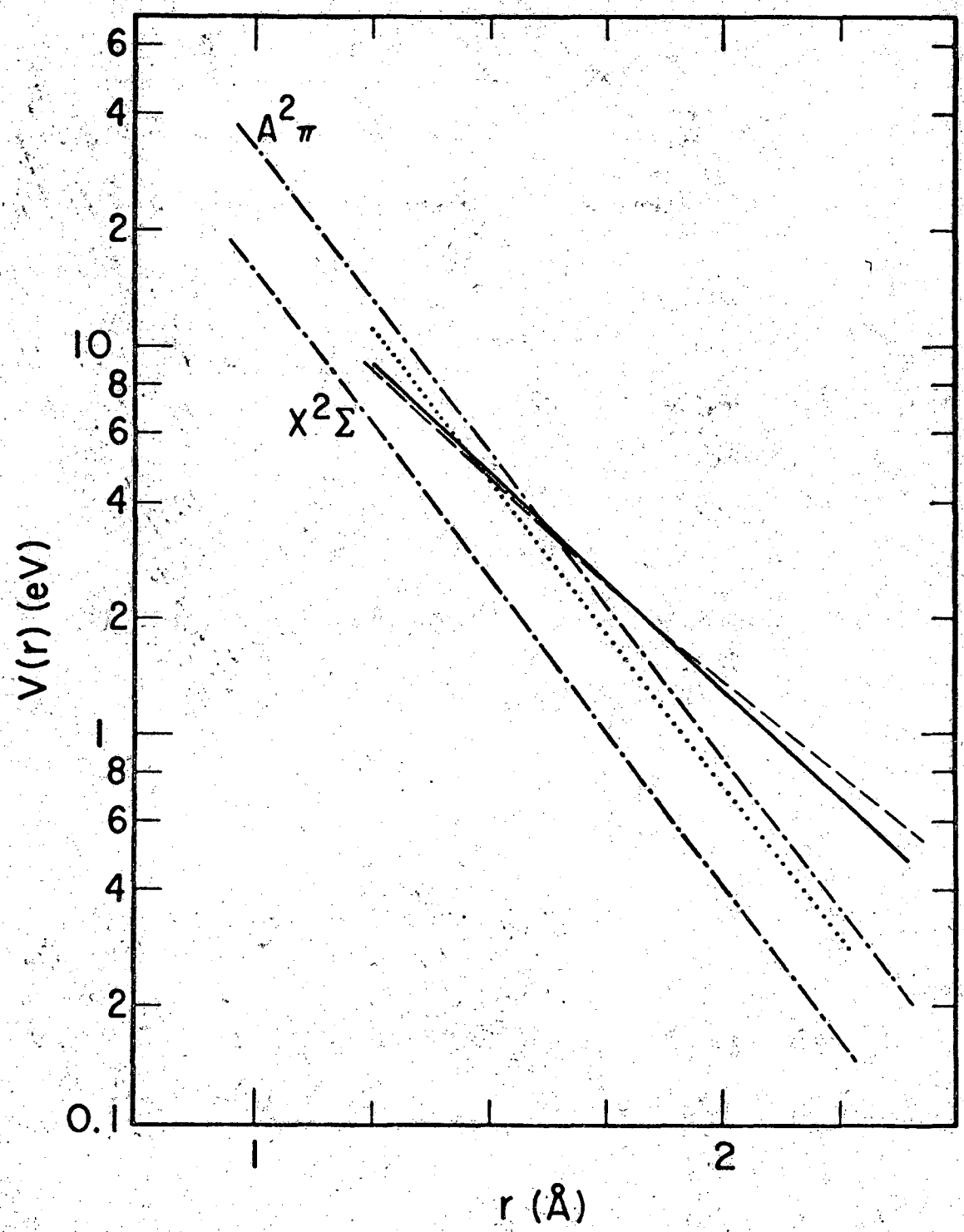

Fig. 5

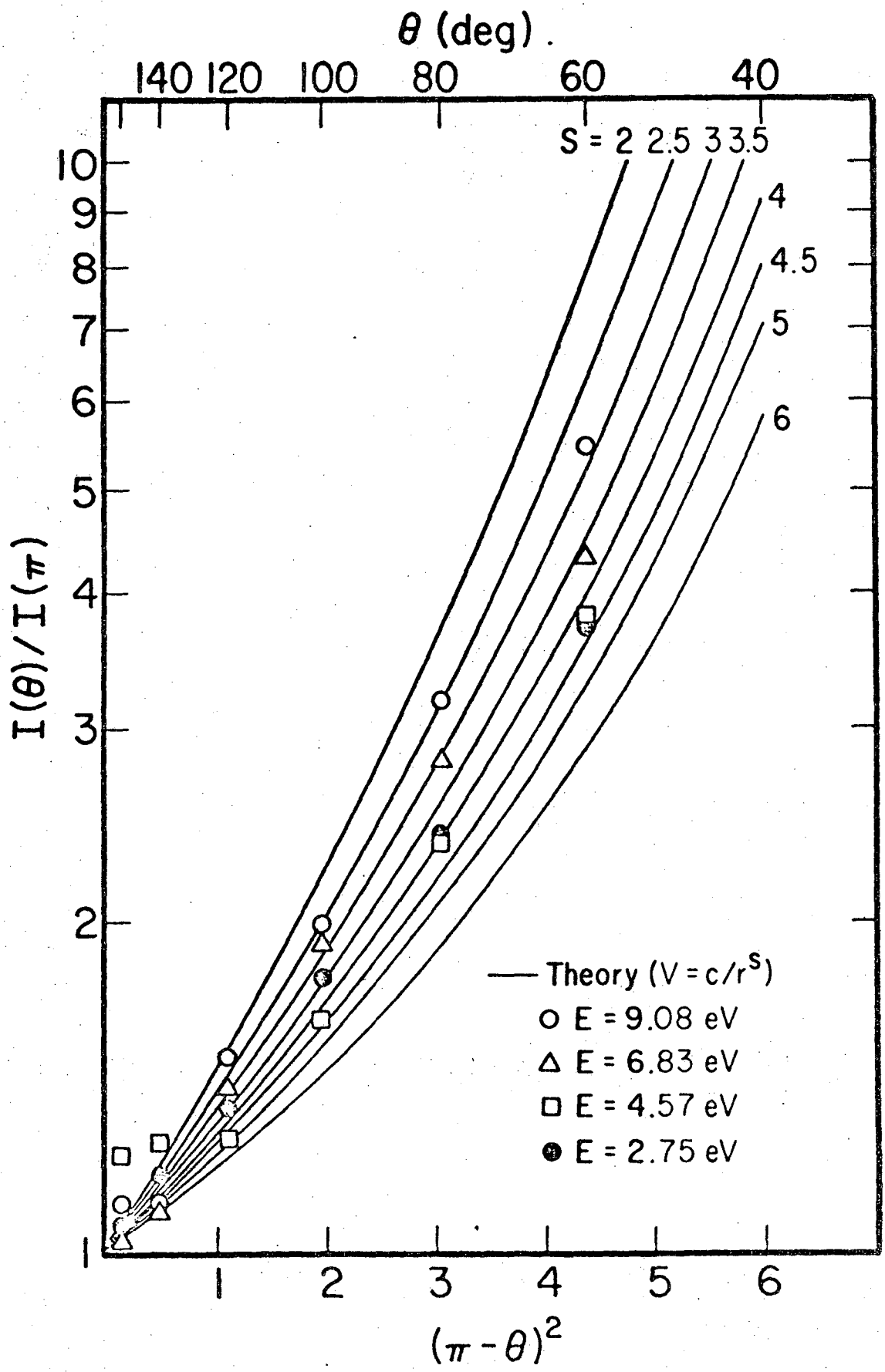
θ (deg)
140 120 100 80 60 40
S = 2 2.5 3 3.5
4
4.5
5
6
10
9
8
7
6
5
4
3
2
1
I(θ)/I(π)
Theory (V = c/r^S)
E = 9.08 eV
E = 6.83 eV
E = 4.57 eV
E = 2.75 eV
1 2 3 4 5 6
(π − θ)^2

Fig. 6

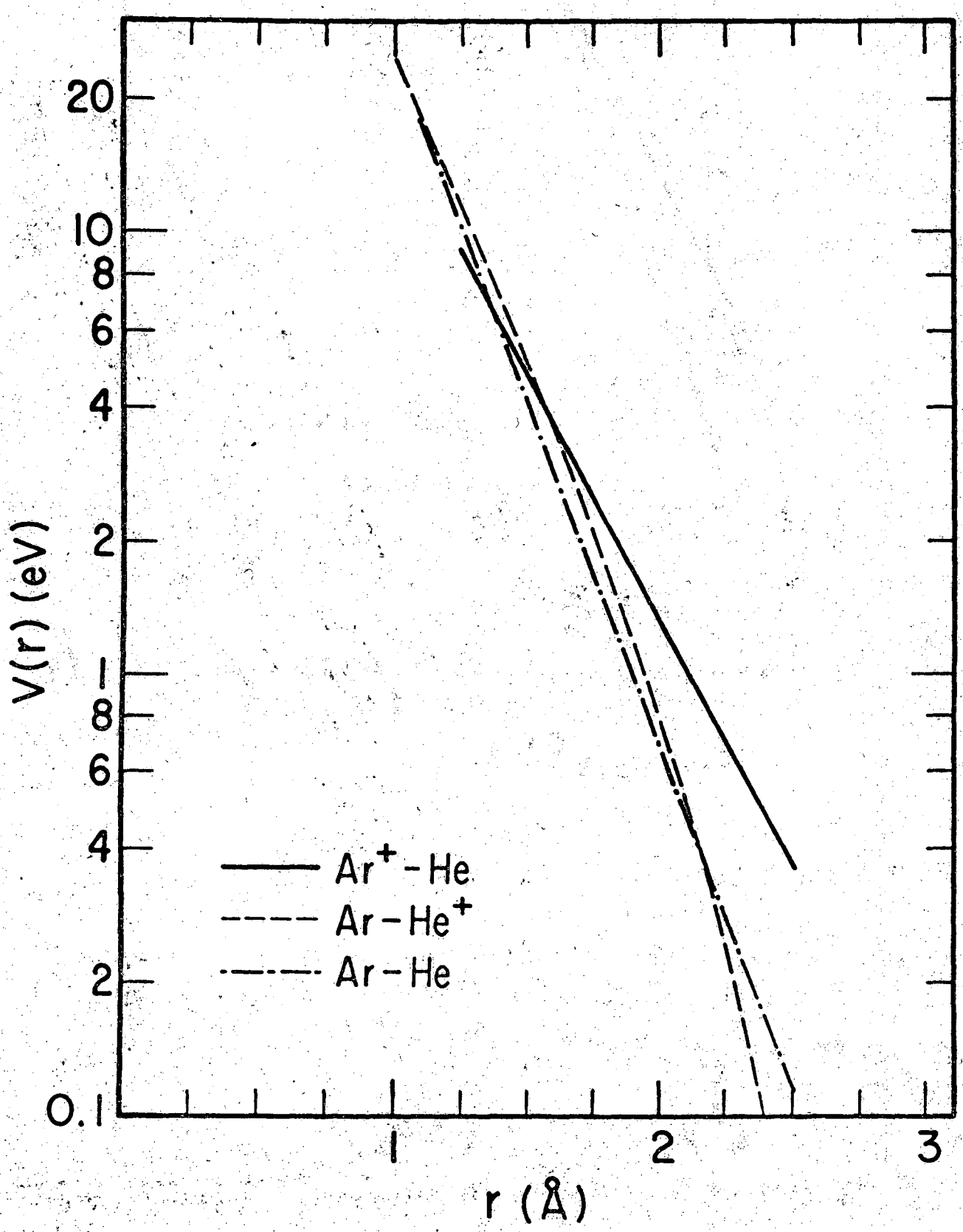

Fig. 7

LEGAL NOTICE

This report was prepared as an account of work sponsored by the United States Government. Neither the United States nor the United States Atomic Energy Commission, nor any of their employees, nor any of their contractors, subcontractors, or their employees, makes any warranty, express or implied, or assumes any legal liability or responsibility for the accuracy, completeness or usefulness of any information, apparatus, product or process disclosed, or represents that its use would not infringe privately owned rights.

TECHNICAL INFORMATION DIVISION
LAWRENCE RADIATION LABORATORY
UNIVERSITY OF CALIFORNIA
BERKELEY, CALIFORNIA 94720